Electron. Mater. Lett., Vol. 12, No. 6 (2016), pp. 753-760
DOI: 10.1007/s13391-016-6224-9

Enhanced Photoelectrochemical Water Splitting and Photocatalytic Water Oxidation of Cu_2O Nanocube-Loaded $BiVO_4$ Nanocrystal Heterostructures

Wenzhong Wang,[1,*] Weiwei Zhang,[1] Shan Meng,[1] Lujie Jia,[1] Miao Tan,[1] Chenchun Hao,[1] Yujie Liang,[1] Jun Wang,[2] and Bin Zou[1]

[1]School of Science, Minzu University of China, Beijing 100081, China
[2]Faculty of Sciences, Ningbo University, Zhejiang, Ningbo 315211, China

(received date: 17 July 2016 / accepted date: 30 August 2016 / published date: 10 November 2016)

Reducing the fast recombination of photogenerated electron-hole pairs of semiconductor photocatalyst is very important to improve its photocatalysis. In this paper we fabricate Cu_2O nanocube-decorated $BiVO_4$ nanocrystal (denoted as $BiVO_4$@Cu_2O nanocrystal@nanocube) heterostructure photocatalyst by coupling *n*-type $BiVO_4$ with *p*-type Cu_2O. The $BiVO_4$@Cu_2O nanocrystal@nanocube photocatalysts show superior photocatalytic activities in photoelectrochemical (PEC) activity and photocatalytic water oxidation to $BiVO_4$ photocatalysts under visible light illumination. The $BiVO_4$@Cu_2O nanocrystal@nanocube heterostructure electrode achieves the highest photocurrent density of ~ 10 μA cm^{-2} at 0 V versus Ag/AgCl, 5 times higher than that of $BiVO_4$ nanocrystal electrode (~ 2 μA cm^{-2}). The light induced evolution rate of O_2 generation for $BiVO_4$@Cu_2O nanocrystal@nanocube heterostructures is as high as 150 μmol h^{-1}100 mg cat^{-1}, more than 3 times higher than that (48 μmol h^{-1}100 mg cat^{-1}) of $BiVO_4$ nanocrystals. The enhanced photocatalysis activities of the $BiVO_4$@Cu_2O nanocrystal@nanocube photocatalysts are attributed to the efficient separation of the photoexcited electron-hole pairs caused by inner electronic field (IEF) of *p-n* junction. This study opens up new opportunities in designing photoactive materials with highly enhanced performance for solar energy conversion.

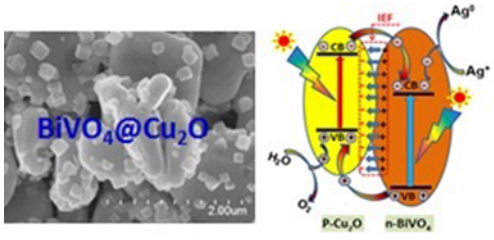

Keywords: nanocrystals, *p-n* junction heterostructures, photoelectrochemical performance, water oxidation, visible light

1. INTRODUCTION

Recently, numerous studies have demonstrated that semiconductor photocatalytic technique based on solar light is widely considered as one of the most promising ways to provide a sustainable energy source in the future.[1-3] Semiconductor-based photocatalytic water splitting has been generally considered as one efficient option for economic conversion of solar to chemical energy.[4-6] Among semiconductor photocatalysts, visible-light-driven semiconductor oxide photocatalysts for photocatalytic water splitting have especially attracted considerable interest in recent years, due to their capability to convert solar energy to chemical energy by direct use of sunlight.[7-9] In addition, many studies on photocatalytic performance of semiconductor oxide photocatalysts have shown that the conversion efficiency of solar to chemical energy is heavily determined from efficient separation of the photogenerated electron-hole pairs in photocatalyst. However, it has been demonstrated that almost every oxide semiconductor photocatalyst has a high recombination rate of the photoinduced electron-hole pairs.[10,11] Therefore, considerable attempts have been devoted to addressing this problem through fabricating heterogeneous photocatalysts with efficiently photogenerated electron-hole separation and enhanced photocatalysis activity.

It has been demonstrated that heterogeneous photocatalysts fabricated by combining one semiconductor with two or more than two semiconductors have capability of separating photogenerated electron-hole pairs efficiently, leading to enhanced photocatalysis performance.[12,13] Especially, heterogeneous photocatalysts constructed by coupling one

*Corresponding author: wzhwangmuc@163.com

p-type semiconductor with one *n*-type semiconductor are expected to exhibit much high separation efficiency of the photoinduced electron-hole pairs and therefore much higher photocatalytic performance, because the *p*-*n* junction in the interface of *p*-type semiconductor and *n*-type semiconductor creates an internal electric field (IEF) from *n*-type semiconductor to *p*-type semiconductor. Under the effect of the established IEF, the photogenerated electrons and holes migrate to opposite directions, resulting in an efficient separation of the electron-hole pairs and hence a significant enhancement for photocatalytic activity.[14-16] For instance, it was reported that the heterogeneous *p*-*n* junction photocatalyst of *n*-$BiVO_4$/*p*-Co_3O_4 with 0.8 wt.% cobalt showed the significant enhancement for incident-photon-to-current efficiencies, 4 times higher than that of *n*-$BiVO_4$ under illumination with 420 nm.[15] The *p*-*n* junction ZnO/ZnS/CdS/$CuInS_2$ heterostructures formed with *p*-type $CuInS_2$ and *n*-type ZnO/ZnS/CdS showed remarkable improvement for visible light photoelectrocatalytic water splitting performance to ZnO/ZnS/CdS and ZnO/ZnS films.[16] These studies demonstrate that the *p*-*n* junction semiconductor photocatalyst can be a very good candidate for solar water splitting.

As a *n*-type semiconductor, bismuth vanadate ($BiVO_4$) with band gap energy of about 2.45 eV is considered as a potentially suitable visible-light photocatalyst towards water oxidation,[17,18] due to its favorable conduction band (CB) and valence band (VB), and capability to absorb a substantial portion of the visible spectrum.[19] However, several reports have demonstrated that photoexcited electrons and holes are inclined to rapidly recombination in the body of bare $BiVO_4$ crystal, significantly lowered the photocatalytic efficiency.[20,21] Consequently, a key issue for improving the visible-light photocatalytic performance of $BiVO_4$ photocatalyst is to separate its photogenerated electrons and holes efficiently by constructing heterogeneous photocatalytic system.

In this study, we report the fabrication of heterostructure photocatalyst of *p*-Cu_2O nanocube-decorated *n*-$BiVO_4$ nanocrystals (denoted as $BiVO_4$@Cu_2O nanocrystal@nanocube heterostructures) and its enhanced photoelectrochemical (PEC) activity and photocatalytic water oxidation under visible light illumination. A working mechanism was proposed to understand the improved separation of the photogenerated electrons and holes, and the enhanced PEC activity and photocatalytic water oxidation of $BiVO_4$@Cu_2O nanocrystal@nanocube heterostructures.

2. EXPERIMENTAL PROCEDURE

A facilely hydrothermal method has been employed to synthesize $BiVO_4$ nanocrystals. In a typical synthetic procedure, $Bi(NO_3)_3 \cdot 5H_2O$ (2.42 g) was dissolved in HNO_3 (2 mL) under constant stirring, followed by adding 7.5 mL high purity water to form a solution (denoted as solution A). Secondly, NH_4VO_3 (0.58 g) was dissolved in NaOH solution (10 mL, 4 M), followed by adding ethylenediaminetetraacetates (EDTA) (1.00 g) to form a solution (denoted as solution B). Finally, solution B was added into solution A drop by drop, and then the pH of the mixture suspension was adjusted to 7 by slowly adding NaOH solution (2 M). The obtained mixture suspension was subsequently sealed in a 50 mL Teflon-lined stainless-steel autoclave, heated at 180 °C for 24 h.

The $BiVO_4$@Cu_2O nanocrystal@nanocube heterostructures were fabricated by a facile, low cost, and environmental-friendly polyol process. A typical procedure was given as follows: $Cu(CH_3OO)_2 \cdot H_2O$ (80 mg) was dissolved in 50 mL of ethanol (EtOH), then the as-obtained $BiVO_4$ nanocrystals (300 mg) was added to form suspension mixture under sonication. The suspension mixture was stirred for 6 h and subsequently dried to prepare mixture powder of $Cu(CH_3OO)_2 \cdot H_2O$ and $BiVO_4$. Then mixture powder was then suspended in di-ethylene glycol (DEG) solution (180 mL) under sonication to make Cu^{2+} concentration of 2.5 mM, the solution was transferred into a flask with volume of 250 mL and heated at 180 °C for 2 h in an oil bath under stirring.

X-ray powder diffraction (XRD) patterns were recorded on a Rigaku (Japan) Dmax γA rotation anode X-ray diffractometer equipped with graphite monochromatized Cu-Kα radiation (λ = 1.54178 Å), employing a scanning rate of 0.02 ° s^{-1} in the 2θ range from 10 to 80 °. The emission scanning electron microscopy (ESEM) images were taken with a Hitachi S-4800 scanning electron microscope. UV-vis diffuse reflectance spectra (DRS) were recorded on a Lambda 950 UV/vis/NIR spectrophotometer (Perkin-Elmer, USA). X-ray photoelectron spectroscopy (XPS) was carried out on an ESCALAB M KII X-ray photoelectron spectrometer using Mg Kα X-rays as the excitation source, the binding energies obtained in the XPS analysis were corrected with reference to C1s (284.6 eV).

For PEC tests, thin films of $BiVO_4$@Cu_2O nanocrystal@nanocube heterostructures were prepared on a FTO glass electrode (1.0 × 1.0 cm^2) by drop coating and drying at 60 °C in vacuum condition for 6 h. The measurements were conducted on a three-electrode configuration in a quartz cell. The prepared catalyst working electrode was placed into a cell with a Pt counter electrode and Ag/AgCl reference electrode, respectively. The cell was filled with 0.1 M Na_2SO_4 buffer solution (100 mL and pH 7), and the solution was degassed with N_2 for 30 min before illumination. The light source employed in PEC tests was a 300-W Xenon lamp with an AM 1.5 G filter. The linear sweep voltammograms were operated at 5 mVs^{-1} in a potential range from 0.0 to

1.0 V versus Ag/AgCl both in dark and under illumination.

The photocatalytic oxidation of water for O_2 evolution was carried out in a closed gas circulation and evacuation system. Briefly, the as-achieved $BiVO_4$@Cu_2O nanocrystal@nanocube heterostructure catalyst (100 mg) was dispersed in 0.05 M $AgNO_3$ solution (120 mL) to form a suspension in a Pyrex glass reaction cell. The suspension was degassed, and then was illuminated with a 300 W Xenon lamp ($\lambda > 420$ nm) from the top of the cell. During the reaction, the temperature of the solution was kept at room temperature with cooling water. The amount of O_2 was collected and evaluated by an online gas chromatograph.

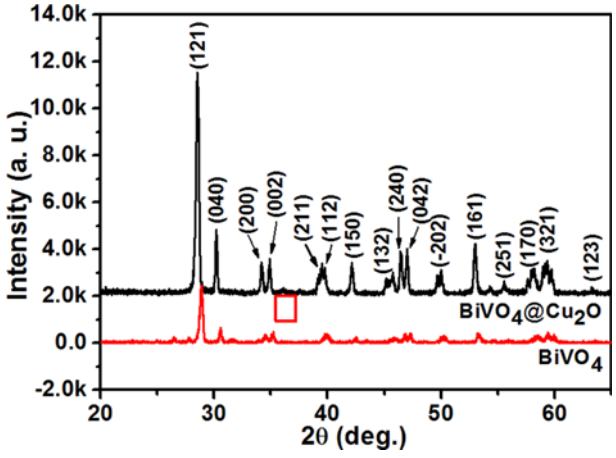

Fig. 1. XRD patterns of the pure $BiVO_4$ nanocrystals and $BiVO_4$@Cu_2O nanocrystal@nanocube heterostructures.

3. RESULTS AND DISCUSSION

The composition and crystal phase of $BiVO_4$ nanocrystals and $BiVO_4$@Cu_2O nanocrystal@nanocube heterostructures was analyzed by XRD as shown in Fig. 1. In the XRD pattern of pure $BiVO_4$ nanocrystals, all diffraction peaks can be easily indexed to those of a monoclinic $BiVO_4$ cell with lattice parameters of a = 5.195 Å, b = 11.701 Å, c = 5.092 Å and β = 90.38 ° (JCPDS No. 14-0668). As for the XRD pattern of the as-achieved $BiVO_4$@Cu_2O nanocrystal@nanocube heterostructures, the dominant diffraction peaks are also from the monoclinic $BiVO_4$ crystallite as shown in Fig. 1, indicating that there is a small portion of Cu_2O nanocrystals in heterogeneous structures. However, a weak diffraction peak located at about 36.5 ° can be obviously detected as demonstrated in Fig. 1. This peak can be easily assigned to the (111) plane of the Cu_2O crystallite, showing the $BiVO_4$@Cu_2O nanocrystal@nanocube heterostructures were achieved in the present work.

SEM was employed to evaluate the morphology and size of $BiVO_4$ nanocrystals and $BiVO_4$@Cu_2O nanocrystal@nanocube heterostructures. SEM images of the $BiVO_4$ nanocrystals reveal that large quantity of plate-like nanocrystals with thickness of about 100 to 400 nm was achieved as shown in Fig. 2 A, B. The surfaces of the $BiVO_4$ nanocrystals are very smooth and clean as clearly shown in Fig. 2B. After depositing reaction, a large number of Cu_2O nanocubes were assembled on the surfaces of plate-like $BiVO_4$ nanocrystals as shown in Fig. 2 C, D. Higher

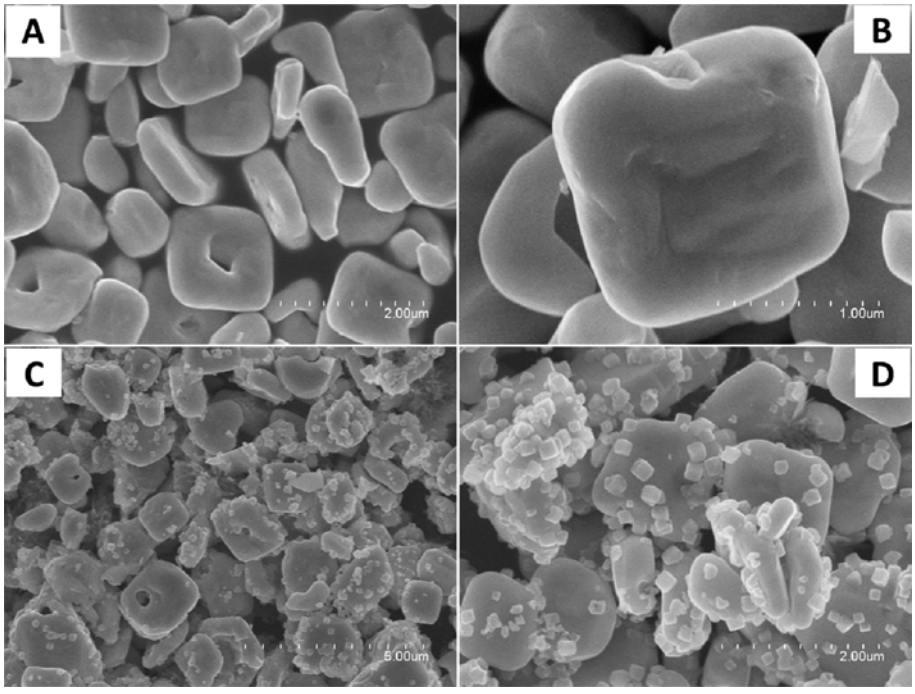

Fig. 2. SEM images of the as-prepared products: (A) and (B) pure $BiVO_4$ nanocrystals with different magnifications, (C) and (D) $BiVO_4$@Cu_2O nanocrystal@nanocube heterostructures with different magnifications.

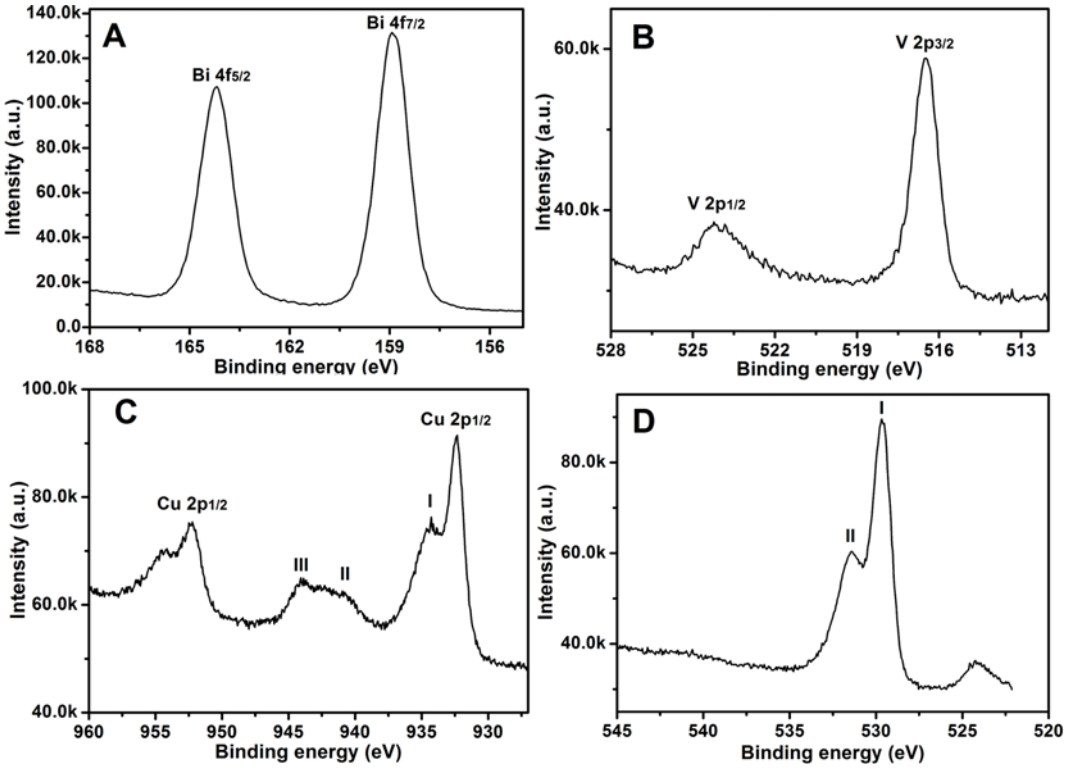

Fig. 3. High-resolution XPS spectra of the as-fabricated $BiVO_4$@Cu_2O nanocrystal@nanocube heterostructures: (A) Bi 4f, (B) V 2p, (C) Cu 2p, and (D) O 1s.

magnification SEM images as presented in Fig. 2D demonstrate that the Cu_2O nanocrystals exhibit cube-like morphology with edge length of about 80 to 100 nm.

XPS has been applied to further analyze the composition and chemical state of elements in $BiVO_4$@Cu_2O nanocrystal @nanocube heterostructures. In the XPS spectrum of Bi 4F band as shown in Fig. 3A, two binding energies at 164.2 and 158.9 eV can be indexed to Bi $4f_{5/2}$ and Bi $4f_{7/2}$ bands, respectively. In Fig. 3B, the binding energies located at 524.2 and 516.4 eV can be assigned to V $2p_{1/2}$ and V $2p_{3/2}$ bands, respectively. Figure 3C shows the high-resolution XPS spectrum of Cu 2p band, in which two binding energies at 952.6 and 932.3 eV correspond to Cu $2p_{1/2}$ and Cu $2p_{3/2}$ bands of Cu_2O crystallites, respectively. In addition, an obvious feature of Cu 2p band is that there are three satellites on the high-binding-energy side of the Cu $2p_{3/2}$ peak. These three satellites locate at 934.2, 940.4, and 943.6 eV, which are denoted as I, II and III peaks (Fig. 3C), respectively. The high-resolution XPS spectrum of Cu 2p demonstrates main characteristics of Cu^+ and the feature of an open $3d^9$ shell of Cu^{2+} state, which is confirmed by shake-up satellite peaks.[22] Thus the XPS spectrum of Cu 2p indicates the presence of CuO at the surface of Cu_2O nanocrystals. It is worthwhile to note that no CuO phase is detected in the XRD pattern of $BiVO_4$@Cu_2O nanocrystal@nanocube heterostructures, suggesting the amount of CuO in the heterostructures is beyond the detection limit of XRD. In the XPS spectrum of O 1s band as shown in Fig. 3D, the binding energies at 529.9 and 531.2 eV (denoted as I and II) are attributed to the O 1s band of lattice oxygen of Cu_2O[23] and $BiVO_4$,[24] respectively. So, it can be concluded that the Cu element exists in the form of Cu_2O on the surface of $BiVO_4$@Cu_2O nanocrystal@ nanocube heterostructures.

It has been reported that the DRS is usually applied to evaluate the band edge of the semicondcutors. For a crystalline semiconductor, the equation $\alpha E_{photon} = K(E_{photon} - E_g)^{n/2}$ has been widely employed to determine the relationship of band edge and optical absorption, where α, E_{photon}, K and E_g are the absorption coefficient, the discrete photo energy, a constant and the band gap energy, respectively.[25] For the direct and indirect semiconductor, the values of n are 1 and 4, respectively. Figure 4 shows the DRS of $BiVO_4$ nanocrystals and $BiVO_4$@Cu_2O nanocrystal@nanocube heterostructures. As reported in previous literature, monoclinic $BiVO_4$ is a direct semiconductor. Thus n value is 1 for $BiVO_4$ crystallite. Because amounts of $BiVO_4$ nanocrystals are the main constituents in $BiVO_4$@Cu_2O nanocrystal@ nanocube heterostructures, the value of the band gap energy of the heterostructures also evaluated by the equation $\alpha E_{photon} = K(E_{photon} - E_g)^{n/2}$ with n value of 1. E_g values of the $BiVO_4$ nanocrystals and $BiVO_4$@Cu_2O nanocrystal@ nanocube heterostructures are estimated from the plot of

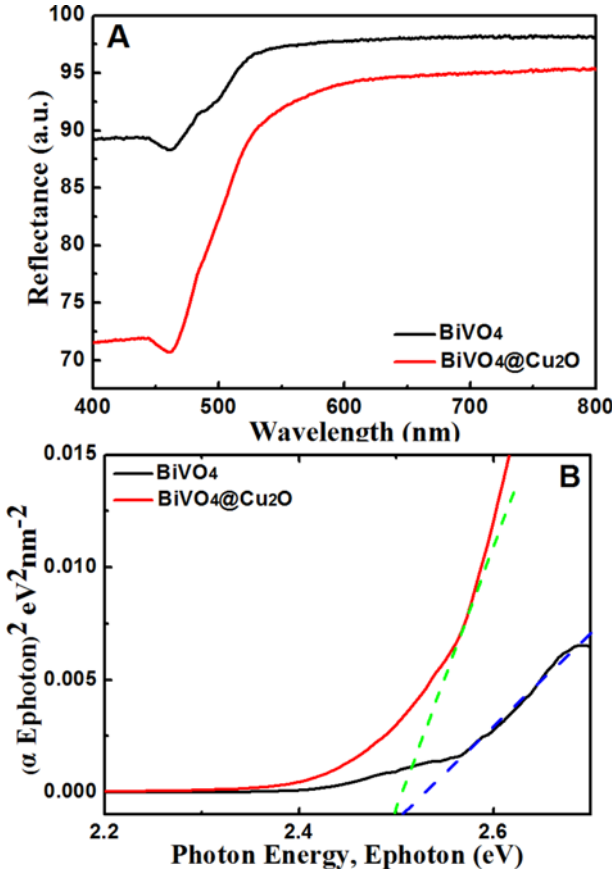

Fig. 4. (A) Diffuse reflectance spectra of $BiVO_4$ nanocrystals and $BiVO_4$@Cu_2O nanocrystal@nanocube heterostructures. (B) Band gap energy of the as-prepared pure $BiVO_4$ nanocrystals and the as-fabricated $BiVO_4$@Cu_2O nanocrystal@nanocube heterostructures.

$(\alpha E_{photon})^2$ vs E_{photon} as shown in Fig. 4B. The absorption edge energies of the $BiVO_4$ nanocrystals and $BiVO_4$@Cu_2O nanocrystal@nanocube heterostructures are 2.48 and 2.46 eV, respectively, evaluated by the extrapolated value (the straight line to the χ axis) of E_{photon} at $\alpha = 0$.

To evaluate whether the as-fabricated $BiVO_4$@Cu_2O nanocrystal@nanocube heterostructures show enhanced PEC performance under visible illumination, a set of PEC measurements were carried out. Figure 5 shows the chronoamperometric I-t curves of the $BiVO_4$ nanocrystal and $BiVO_4$@Cu_2O nanocrystal@nanocube heterostructure electrode, recorded in 0.1 M Na_2SO_4 electrolyte in the dark and under visible light illumination ($\lambda > 420$ nm) at 0 V versus Ag/AgCl. The $BiVO_4$@Cu_2O nanocrystal@nanocube heterostructure electrode achieves the highest photocurrent density of 10 μA cm^{-2} at 0 V versus Ag/AgCl, 5 times higher of the photocurrent density for bare $BiVO_4$ nanocrystal electrode (2 μA cm^{-2}). It has been reported that I-t property obtained by PEC activity can reveal the interfacial generation and separation dynamics of photogenerated charges for semiconductor photocatalyst. A larger photocurrent indicates

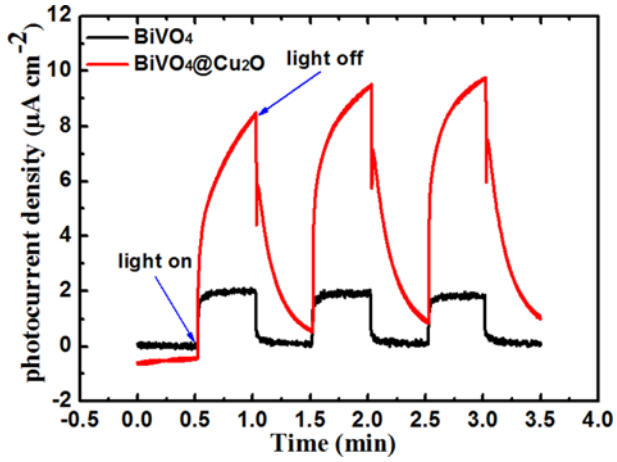

Fig. 5. Amperometric *I-t* curves at 0 V versus Ag/AgCl under illumination of visible light with wavelength ≥ 420 nm with 60 s light on/off cycles.

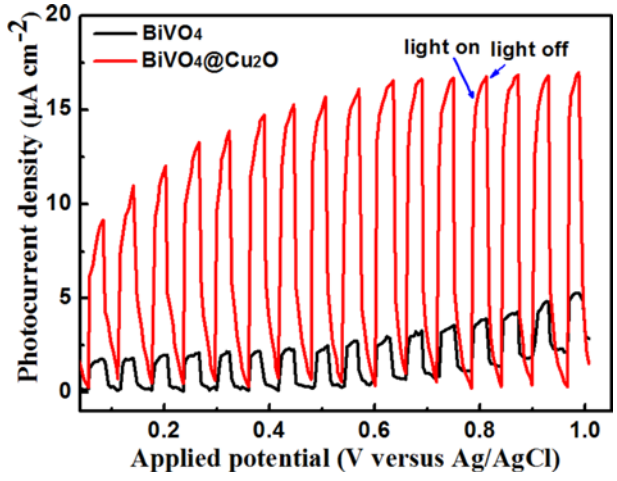

Fig. 6. Photocurrent density versus applied potential curves under chopped 300 W Xe lamp irradiation, recorded at 5 mVs^{-1} and pH = 7 in 0.1 M Na_2SO_4 buffer solution.

higher electrons and holes separation efficiency.[26] Thus the enhanced photocurrent density on the $BiVO_4$@Cu_2O nanocrystal@nanocube heterostructure is ascribed to its higher electrons and holes separation efficiency. In addition, when the light was turned off, the residual current (dark current) of Cu_2O nanocube-loaded $BiVO_4$ nanocrystal photoanode did not approach to zero rapidly, compared to pure $BiVO_4$ nanocrystal photoanode. This result suggested that Cu_2O nanocube-loaded $BiVO_4$ nanocrystal heterostructures was able to carry out direct electrochemical redox reaction, as reported in previous literature.[27]

Figure 6 shows a set of linear sweep voltammagrams (LSV) of $BiVO_4$ nanocrystal and $BiVO_4$@Cu_2O nanocrystal @nanocube heterostructure electrodes under visible light illumination, recorded in 0.1 M Na_2SO_4 buffer solution at pH 7 and at 5 mVs^{-1} in a potential range from 0.0 to 1.0 V versus

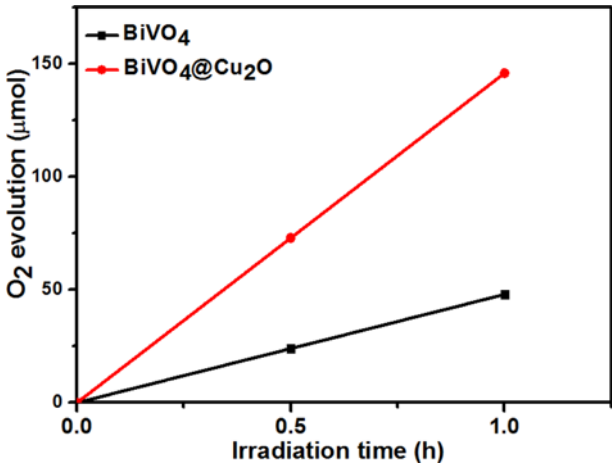

Fig. 7. The amount of oxygen evolution versus visible light (λ > 420 nm) irradiation time through photocatalytic water oxidation by using $BiVO_4$ and $BiVO_4$@Cu_2O nanocrystal@nanocube heterostructures in the presence of sacrificial agent $AgNO_3$.

Ag/AgCl, both in dark and under illumination with a 300 W Xenon lamp (AM 1.5G, 100 mW/cm^2). The LSVs clearly demonstrate that the $BiVO_4$@Cu_2O nanocrystal@nanocube heterostructure photoelectrode exhibits fast light response, due to efficient charge separation and transport through *p-n* junctions. At 0.96 V versus Ag/AgCl, the photocurrent density generated on the pure $BiVO_4$ nanocrystal photoelectrode is ~3.0 μA cm^{-2}, while the one on the $BiVO_4$@Cu_2O nanocrystal@nanocube heterostructure photoelectrode is ~22.0 μA cm^{-2}, more than 7 times higher than that for pure $BiVO_4$ nanocrystal photoelectrode. Thus the remarkable photocurrent density enhancement in the LSVs further confirms that the as-constructed $BiVO_4$@Cu_2O nanocrystal @nanocube heterostructures show enhanced PEC activity, compared to the pure $BiVO_4$ nanocrystals.

We further study photocatalytic water oxidation for O_2 evolution of $BiVO_4$@Cu_2O nanocrystal@nanocube heterostructures and $BiVO_4$ nanocrystals under visible light (λ > 420 nm) illumination in the presence of sacrificial electron acceptor $AgNO_3$. As shown in Fig. 7, the light induced evolution rate of O_2 generation for $BiVO_4$@Cu_2O nanocrystal @nanocube heterostructures is as high as 150 μmol h^{-1} 100 mg cat^{-1}, which is more than 3 times higher than that (48 μmol h^{-1}100 mg cat^{-1}) of pure $BiVO_4$ nanocrystals. This further confirms the high visible-light photocatalytic efficiency of the $BiVO_4$@Cu_2O nanocrystal@nanocube heterostructures, compared to the pure $BiVO_4$ nanocrystals.

As is well documented in the previous literature, in the heterostructure formed with *p*-type and *n*-type semiconductor, there is a space charge region caused by the opposite direction diffusion of electrons in *n*-type semiconductor and holes in *p*-type semiconductor, leading to a *p-n* junction at the interface of semiconductors and an IEF from *n*-type semiconductor to *p*-type semiconductor. The built IEF can significantly separate the photoexcited electrons and holes of the semiconductor heterostructures, leading to enhanced photocatalytic performance. In the present work, Cu_2O is a *p*-type semiconductor with direct band gap of ca. 2.0 eV,[28] $BiVO_4$ is a *n*-type semiconductor with a band gap of ca 2.45 eV.[19,29] Hence the $BiVO_4$@Cu_2O nanocrystal@nanocube heterostructures are expected to show enhanced PEC activity, compared to pure $BiVO_4$ nanocrystals.

The understanding of the charge separation process between *p*-type Cu_2O and *n*-type $BiVO_4$ is very important to elucidate the enhanced photocatalysis performance and PEC activity of the $BiVO_4$@Cu_2O nanocrystal@nanocube heterostructures. Thus the construction of an energy diagram between *p*-type Cu_2O and *n*-type $BiVO_4$ by their CB and VB positions is a key issue to illustrate the transfer and separation of the photoexcited electrons and holes in the system. As reported in the previous literature, the CB and VB positions of a semiconductor can be calculated by the following equations:[30]

$$E_{VB} = X - E^e + 0.5E_g \quad (1)$$

$$E_{CB} = E_{VB} - E_g \quad (2)$$

Wherein, X, E^e and E_g are the absolute electronegativity of the semiconductor, the energy of free electrons on the hydrogen scale (ca. 4.5 eV) and the band gap of the semiconductor, respectively. The X values for Cu_2O and $BiVO_4$ are ca. 4.84 eV[31] and 6.035 eV,[32] respectively. The E_g values for Cu_2O and $BiVO_4$ are ca. 2.0 eV[29] and 2.45 eV,[19] respectively. The calculated VB and CB values of *p*-type Cu_2O are 1.3 and −0.7 eV, respectively. While the VB and CB values of *n*-type $BiVO_4$ are calculated to be 2.76 and 0.31 eV, respectively.

According to the VB and CB values of *p*-type Cu_2O and *n*-type $BiVO_4$ semiconductor, before contact of Cu_2O and

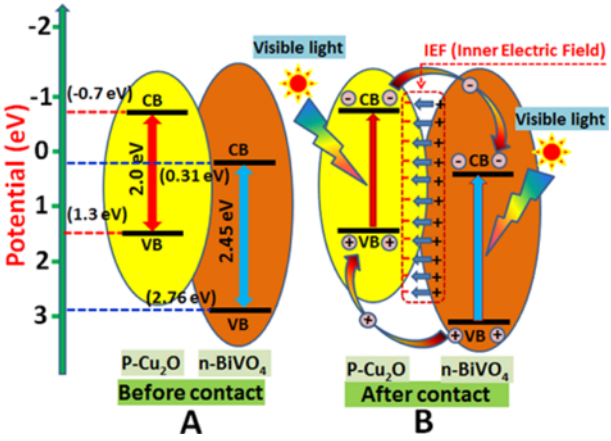

Fig. 8. Schematic energy diagram and charge transfer between *p*-type Cu_2O and *n*-type $BiVO_4$: (A) before contact and (B) after contact to the formation of the *p-n* junction.

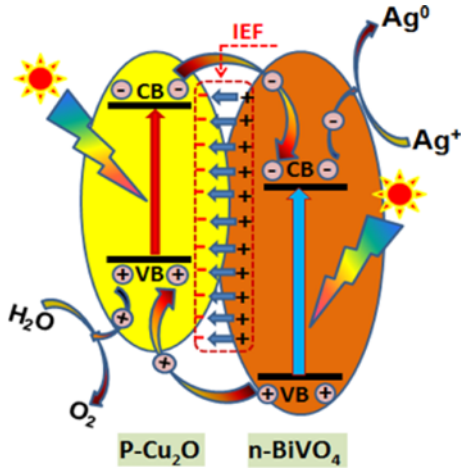

Fig. 9. The proposed mechanism of photocatalytic water oxidation by $BiVO_4$@Cu_2O nanocrystal@nanocube heterostructures in the presence of sacrificial agent $AgNO_3$.

$BiVO_4$, the Fermi level of *p*-type Cu_2O is lower than that of *n*-type $BiVO_4$, and the CB edge of *p*-type Cu_2O is higher than that of *n*-type $BiVO_4$ as demonstrated in Fig. 8A. After contact of Cu_2O and $BiVO_4$, with the Fermi level move up and down of *p*-type Cu_2O and *n*-type $BiVO_4$, respectively, an equilibrium state is established in *p*-type Cu_2O/*n*-type $BiVO_4$ heterostructure as shown in Fig. 8B. Meanwhile, the whole energy band of Cu_2O is raised up with the move up of its Fermi level, while whole energy band of $BiVO_4$ is descended with the move down of its Fermi level. As a result, the CB edge of Cu_2O is much higher than that of $BiVO_4$, while the VB of $BiVO_4$ is much lower than that of Cu_2O, leading to an IEF from *n*-type $BiVO_4$ to *p*-type Cu_2O at the equilibrium as shown in Fig. 8B. The energy-band schematic diagram of the $BiVO_4$@Cu_2O nanocrystal@nanocube heterostructure is shown in Fig. 8.

In the as-constructed $BiVO_4$@Cu_2O nanocrystal@nanocube heterostructure, both Cu_2O and $BiVO_4$ can be excited by visible-light to generate electrons and holes. As demonstrated in the above energy-band schematic diagram (Fig. 8B), when both Cu_2O and $BiVO_4$ are irradiated with visible light, the photoexcited electrons on the CB of the *p*-type Cu_2O can transfer to that of the *n*-type $BiVO_4$, and holes remain in the VB of *p*-type Cu_2O, while the photoinduced holes on the VB of *n*-type $BiVO_4$ can migrate to that of *p*-type Cu_2O, the photogenerated electrons remain in the CB of *n*-type $BiVO_4$ as shown in Fig. 8B. In addition, the migration of the photoexcited electrons and holes in the $BiVO_4$@Cu_2O nanocrystal@nanocube heterostructure can be significantly promoted by the established IEF, which is from *n*-type $BiVO_4$ to *p*-type Cu_2O. Hence the photoexcited electrons and holes in the $BiVO_4$@Cu_2O nanocrystal@nanocube heterostructure can be separated efficiently by the *p*-*n* junction formed between the *p*-type Cu_2O and *n*-type $BiVO_4$ interface, and the recombination of electron-hole pairs can be significantly reduced.

The effective separation of photogenerated electrons and holes in the $BiVO_4$@Cu_2O nanocrystal@nanocube heterostructure are responsible for its improved PEC performance for water oxidation. When the $BiVO_4$@Cu_2O nanocrystal@nanocube heterostructure on the working electrode was irradiated by visible light, the photoexcited electrons migrate to the counter electrode and holes remain in the working electrode, resulting in the generation of photocurrent. As analyzed above, the IEF built in the $BiVO_4$@Cu_2O nanocrystal@nanocube heterostructure can accelerate the transfer of photoexcited electrons from *p*-type Cu_2O to *n*-type $BiVO_4$ and the migration of the photoexcited holes from *n*-type $BiVO_4$ to *p*-type Cu_2O, causing significantly enhanced amount of the electrons in the counter electrode, and resulting in the photocurrent enhancement to pure $BiVO_4$.

According to the energy alignment of the $BiVO_4$@Cu_2O nanocrystal@nanocube heterostructure as shown in Fig. 8B, for the photogenerated electrons and holes in *p*-type Cu_2O, the electrons on the CB of Cu_2O will transfer to that of $BiVO_4$, while holes remain on the VB of Cu_2O. For the photogenerated electrons and holes in *n*-type $BiVO_4$, the holes on the VB of $BiVO_4$ will transfer to that of Cu_2O, while the electrons remain on the CB of $BiVO_4$, leading to the efficient separation of the photogenerated electrons and holes in heterostructure, and thereby increasing their lifetime.[33] Increasing lifetime of photogenerated charges is very important to photocatalytic water oxidation because it is slow multielectron processes.[34] When the photoexcited electrons on the surface of *n*-type $BiVO_4$ reduce the adsorbed Ag^+ to Ag^0, the holes on the surface of *n*-type Cu_2O will have relatively longer lifetime to carry out the four-electron process of H_2O oxidation to O_2. The proposed mechanism of photocatalytic water oxidation by $BiVO_4$@Cu_2O nanocrystal@nanocube heterostructures in the presence of sacrificial agent $AgNO_3$ is illustrated in Fig. 9.

4. CONCLUSIONS

We report that the appropriate energy level match between *p*-type Cu_2O nanocubes and *n*-type $BiVO_4$ nanocrystals makes it to establish *p*-*n* junction at the interface, prompting the highly efficient separation of the photogenerated electron-hole pairs and subsequently leading to the remarkably enhanced photocatalysis activity. The as-constructed *p*-*n* junction $BiVO_4$@Cu_2O nanocrystal@nanocube heterostructure photocatalysts show superior activity in both PEC activity and photocatalytic water oxidation under visible irradiation. The $BiVO_4$@Cu_2O nanocrystal@nanocube heterostructure electrode achieves the highest photocurrent density of 10 μA cm^{-2} at 0 V versus Ag/AgCl, 5 times higher than that of bare

$BiVO_4$ nanocrystal electrode (2 μA cm^{-2}). The photocurrent density generated on $BiVO_4$@Cu_2O nanocrystal@nanocube heterostructure electrode is up to 22 μA cm^{-2}, more than 7 times higher than that (3.0 μA cm^{-2}) of pure $BiVO_4$ nanocrystal electrode at 0.96 V versus Ag/AgCl. The light induced evolution rate of O_2 generation for $BiVO_4$@Cu_2O nanocrystal@nanocube heterostructures is as high as 150 μmol h^{-1}100 mg cat^{-1}, which is more than 3 times higher than that (48 μmol h^{-1}100 mg cat^{-1}) of pure $BiVO_4$ nanocrystals. We believe that this study can have considerable impact on the future development of highly efficient visible-light *p-n* junction photocatalysts with highly enhanced performance for solar energy conversion.

ACKNOWLEDGEMENTS

This work was supported by the National Natural Science Foundation of China under Grant Nos 11074312, 61575225, 11374377, 11474174 and 11404414), and the Undergraduate Research Training Program of Minzu University of China under Grant Nos.URTP2015110009 and URTP2015110010.

REFERENCES

1. X. Chen, S. Shen, L. Guo, and S. S. Mao, *Chem. Rev.* **111**, 6503 (2010).
2. A. Paracchino, V. Laporte, K. Sivula, M. Gratzel, and E. Thimsen, *Nat. Mater.* **10**, 456 (2011).
3. M. G. Walter, E. L. Warren, J. R. McKone, S. W. Boettcher, Q. Mi, E. A. Santori, and N. S. Lewis, *Chem. Rev.* **111**, 6446 (2010).
4. H. S. Kim, K.-S. Ahn, and S. H. Kang, *Electron. Mater. Lett.* **10**, 345 (2014).
5. Y. J. Lin, S. Zhou, S. W. Sheehan, and D. W. Wang, *J. Am. Chem. Soc.* **133**, 2398 (2011).
6. A. Yamaguchi, R. Inuzuka, T. Takashima, T. Hayashi, K. Hashimoto, and R. Nakamura, *Nat. Commun.* **5**, 4256 (2014).
7. Y. H. Pu, G. M. Wang, K. D. Chang, Y. C. Ling, Y. K. Lin, B. C. Fitzmorris, C. M. Liu, X. H. Lu, Y. X. Tong, J. Z. Zhang, Y. J. Hsu, and Y. Li, *Nano Lett.* **13**, 3817 (2013).
8. X. F. Zhang, Y. Gong, X. L. Dong, X. X. Zhang, C. Ma, and F. Shi, *Mater. Chem. Phys.* **136**, 472 (2012).
9. Y. H. Ng, A. Iwase, A. Kudo, and R. Amal, *J. Phys. Chem. Lett.* **1**, 2607 (2010).
10. A. L. Linsebigler, G. Lu, and J. T. Yates, *Chem. Rev.* **95**, 735 (1995).
11. D. B. Ingram and S. Linic, *J. Am. Chem. Soc.* **133**, 5202 (2011).
12. Y. Lin, Y. Xu, M. T. Mayer, Z. I. Simpson, G. McMahon, S. Zhou, and D. Wang, *J. Am. Chem. Soc.* **134**, 5508 (2012).
13. S. Mandati, B. V. Sarada, S. R. Dey, and S. V. Joshi, *Electron. Mater. Lett.* **11**, 618 (2015).
14. J. T. Li, F. K. Meng, S. Suri, W. Q. Ding, F. Q. Huang, and N. Q. Wu, *Chem. Commun.* **48**, 8213 (2012).
15. M. Long, W. M. Cai, and H. Kisch, *J. Phys. Chem. C* **112**, 548 (2008).
16. Y. X. Yu, W. X. Ouyang, Z. T. Liao, B. B. Du, and W. D. Zhang, *ACS Appl. Mater. Interfaces* **6**, 8467 (2014).
17. Y. Park, K. J. McDonald, and K. S. Choi, *Chem. Soc. Rev.* **42**, 2321 (2013).
18. T. W. Kim and K. S. Choi, *Science* **343**, 990 (2014).
19. A. Kudo, K. Omori, and H. Kato, *J. Am. Chem. Soc.* **121**, 11459 (1999).
20. F. F. Abdi and R. van de Krol, *J. Phys. Chem. C* **116**, 9398 (2012).
21. D. K. Zhong, S. Choi, and D. R. Gamelin, *J. Am. Chem. Soc.* **133**, 18370 (2011).
22. C. K. Wu, M. Yin, S. O'Brien, and J. T. Koberstein, *Chem. Mater.* **18**, 6054 (2006).
23. C. D. Wagner, W. M. Riggs, L. E. Davis, J. E. Moulder, and G. E. Muilenber, *Handbook of X-ray Photoelectron Spectroscopy,* Perkin-Elmer Corporation Physical Electronics Division, USA (1979).
24. H. Q. Jiang, H. Endo, H. Natori, M. Nagai, and K. Kobayashi, *Mater. Res. Bull.* **44**, 700 (2009).
25. Y. Ohko, K. Hashimoto, and A. Fujishima, *J. Phys. Chem.* A **101**, 8057 (1997).
26. Y. M. He, J. Cai, T. T. Li, Y. Wu, H. J. Lin, L. H. Zhao, and M. F. Luo, *Chem. Eng. J.* **215-216**, 721 (2013).
27. X. Nie, J. Y. Chen, G. Y. Li, H. X. Shi, H. J. Zhao, P. K. Wong, and T. C. An, *J. Chem. Technol. Biotechnol.* **88**, 1488 (2013).
28. P. He, X. Shen, and H. Gao, *J. Colloids Interface Sci.* **284**, 510 (2005).
29. P. Chatchai, Y. Murakami, S. Y. Nosaka, A. Y. Kishioka, and Y. Nosaka, *Electrochim. Acta* **54**, 1147 (2009).
30. H. Xu, H. Li, C. Wu, J. Chu, Y. Yan, H. Shu, and Z. Gu, *J. Hazard. Mater.* **153**, 877 (2008).
31. W. Y. Yang and S. W. Rhee, *Appl. Phys. Lett.* **91**, 232907 (2007).
32. M. C. Long, W. M. Cai, J. Cai, B. X. Zhou, X. Y. Chai, and Y. H. Wu, *J. Phys. Chem. B* **110**, 20211 (2006).
33. V. Subramanian, E. E. Wolf, and P. V. Kamat, *J. Am. Chem. Soc.* **126**, 4943 (2004).
34. J. W. Tang, J. R. Durrant, and D. R. Klug, *J. Am. Chem. Soc.* **130**, 13885 (2008).